Paper No. 115

"THE ROLE OF WAX BLENDS IN RUBBER"

by Thomas M. Knowles* and Michael J. Reynolds

Akron Rubber Development Laboratory
300 Kenmore Boulevard
Akron, OH 44301

Crystal Inc.
601 W. 8th Street
Lansdale, PA 19446-0950

Presented at a meeting of the

Rubber Division, American Chemical Society

Detroit, Michigan

October 17-20, 1989

* Speaker

THE ROLE OF WAX BLENDS IN RUBBER

Thomas M. Knowles

Akron Rubber Development Laboratory, Inc.

Akron, Ohio 44301

AND

Michael J. Reynolds

Crystal, Incorporated

Lansdale, Pennsylvania 19446

INTRODUCTION

Ozone protection has been imparted to rubber vulcanizates for many years by the addition of physical protective agents and chemical antiozonants[1,2,3]. Although ozone was known to cause degradation to rubber vulcanizates since 1926, work in the forties by Newton showed that rubber vulcanizates under stress did not crack due to light, but rather due to ozone[4]. Recognizing that atmospheric ozone attack has a major destructive effect on the surface of rubber under strain, petroleum wax is added by many compounders to their rubber recipes to reduce and control, if not fully eliminate the effects of ozone attack. A characteristic crack formation occurs perpendicular to the direction of strain on non-protected rubber vulcanizates when exposed to ozone.

Generally, there are two major classifications (by molecular structure) of waxes used to protect the rubber surface. The first are the

paraffin waxes, or more properly the normal paraffin (n-paraffin) waxes. These waxes tend to be the most rapid migrators, lower in molecular weight, and linear as compared to the microcrystalline waxes. The paraffin waxes are clearly characterized by their ability to form distinct crystalline surfaces when they congeal. However, this crystallinity leads to higher gas permeability due to film cracking and other discontinuities in use[5]. Thus, a strictly paraffin wax that is also highly crystalline will permit localized cracking at those points where the wax film is discontinuous on the rubber surface.

The second major classification are the nonlinear paraffins (iso-paraffins or cyclo-paraffins) which congeal into an essentially amorphous form and are thus generally called micro-crystalline waxes. These nonlinear waxes control the migration rates, increase the adhesion of the wax film, and improve the film flexibility[6]. The overall combination of paraffin and microcrystalline waxes can minimize the effects of ozone which occur at the rubber surface.

Several theories have developed throughout the years pertaining to ozone protection and experimental evidence supports each theory to some degree[3,7,8,9]. The "Protective Film" theory is one of these and pertains almost exclusively to the waxes, since no chemical reaction will occur between ozone and petroleum wax. Wax protects the surface of the cured rubber materials by virtue of its insolubility in the rubber matrix at the operating temperature of the rubber article. The wax film that forms on the rubber surface, due to this insolubility, acts as a physical barrier to the ozone. This wax film will protect the rubber as long as it remains in a static state. If the surface is disturbed, the wax film may be broken and it must reform if the protection is to be maintained.

Although the absorption of ozone may occur on the rubber surface, it is only when the polymer has exceeded "critical strain" conditions that the cracking becomes pronounced or even catastrophic. Critical strain is defined as the strain at which the onset of ozone attack growth occurs on the surface; no ozone crack growth will occur at any strain less than the critical strain under a given set of conditions[10]. It can be readily surmised that the critical strain conditions will vary from polymer to polymer, compound to compound, and may vary for the same sample due to change in another vital condition such as operating environment (temperature, humidity, ozone concentration, etc.), surface disturbances, and the like. It is therefore very important for any ozone performance analysis to establish the critical strain or strains, or to test throughout a range of strain conditions.

With the increasing complexity in tire and nontire compounding requirements and to more fully understand the role petroleum waxes play in performance, ozone protection, and surface characteristics; a two-variable control composite design was used in our evaluation. The experimental design allowed characterization of each wax's performance as a function of wax concentration and test temperature.

EXPERIMENTAL

Materials

A typical black sidewall-tire compound was used for the evaluation of three different waxes. The recipe is given in Table I. One production size batch (125 Kg) was banbury-mixed at a commercial production facility and kept under refrigeration until further use. The masterbatch was then divided into portions and mixed with the appropriate amount of wax in a

size B banbury. The cure characteristics were determined on the Monsanto curemeter at 160°C for the control and each wax formulation. Samples of each composition were compression molded for 7.5 minutes at 160°C.

Wax Chemical Composition

Three different petroleum waxes varying in paraffin/micro-crystalline ratios were used in this study. Physical properties of each wax were measured and are given in Tables II and III. The Differential Scanning Calorimetry (DSC) data was obtained on a DuPont 9900 Model. The temperature range was 0-100°C at a heating rate of 10°C/min. Differential Thermal Analysis (DTA) was performed on DuPonts' Model 1090. The temperature range was 25-100°C at a heating rate of 10°C/min. The molecular weight distribution of the paraffin portion of each wax was determined using Perkin Elmers' Model 8400 Gas Chromatograph. A 10m, 0.53 mm Sepcol's column was used. Helium was the carrier gas at 0.193 MPa. The oven conditions were 200 to 320°C at 10°C/min. The data was integrated on PE Nelson's Chromatrography 2600 software.

Experimental Design

A two-variable control composite design was used in this evaluation. The experimental design allowed a complete characterization of each wax as a function of wax concentration and test temperature. The design matrix used in our study is shown in Table IV. The ozone test data was then subjected to regression analysis to provide regression equations of the type:

$$Y + A_0 + A_1X_1 + A_2X_2 + A_{12}X_1X_2 + A_{11}X_1^2 + A_{22}X_2^2, \qquad (1)$$

where Y is the predicted time (hours) when ozone cracks appear. X_1 is the ozone test temperature in °C. X_2 is the wax concentration in phr, and the A

coefficients are determined after the results are obtained.

The coded levels (0 +/- 1.414) shown in Table IV are statistically determined and therefore fixed for the experimental design to maintain the integrity of the analysis and results. This design also allows for a systematic and scientific expansion in the future without sacrificing loss of the work performed using this design. Two separate studies were made over a two year time period. Experiments 1-10 were first performed, and later experiments 11-17 were added and carried out to increase the accuracy of the regression equations.

All experimental runs were performed randomly on the control formulation and formulations containing waxes A-C. Only one level (2.25 phr) of wax for bloom testing and surface composition was used.

Bloom Analysis

The experimentation was conducted on the control formulation and the formulations containing 2.25 of wax. From each recipe, ten rubber strips were cut using a 25 x 150 mm die with mylar still present on the ASTM plaque. Two sample strips from each formulation were tested at temperatures of -20, -7.6, 22.5, 52.6, and 65^{o}C at six different time periods. The method used to calculate the amount of wax which migrated to the surface was determined by a hot solvent wash. This was performed after 1, 3, 6, 11 and 21 days. The amount of wax present on the surface was calculated by subtracting the amount of material present on the control from the amount of material present on the formulation being evaluated. After surface area measurements were made, the theoretical thickness of wax formation was calculated. The solvent washed surface ingredients were then subjected to gas chromatrography analysis. The weight percentage of the

paraffin portion of the waxes were plotted as a function of carbon number at the different test temperatures. With the data presented in this manner, one can observe the change in carbon distribution occurring on the rubber surface at a specified temperature over time.

Ozone Testing - Annulus Method

The annulus specimens were cut from the ASTM compression molded test sheets. The specimens were then stretched as a band over a mounting rack which consisted of two 12.7 mm aluminum rods spaced in such a way that the circumference of the inner diameter is equal to the circumference of the outer diameter. Due to the dimensions of the annulus specimens, the stretch induced in the ring provides a strain gradient from 100% at the inside diameter to 0% at the outside diameter. Following the removal of the rack containing the stretched annulus, a calibrated template was used to determine the amount of ozone cracking which had occurred. A rating of 100 would mean no ozone cracking occurred. A rating of 0 would mean that the specimen broke off the mounting rack. The results were then inverted (i.e. 75 becomes 25) so that the data could be statistically treated.

All the formulations were exposed to 50 mPa ozone according to the two composite design test parameters shown in Table IV. Two annulus test specimens were tested for each formulation at each temperature. After samples were placed on the mounting rack, they were then preconditioned for 24 hours at the temperature at which they were going to be exposed to ozone, in an ozone-free chamber. After ozone exposure, samples were rated every two hours. At the day's end, samples would be placed in an ozone free aging chamber until the next day so that the two hour rating could be continued until 24 hours. Thereafter, ratings were made at 48 and 72

hours. Two ratings were made on each of the annulus test specimens. Thus, four ozone crack ratings were obtained for each formulation at a given set of conditions.

The "dynamic" ozone testing was performed exactly the same as the static with one exception. Just prior to ozone exposure, the mounting rack used to hold the annulus specimens in place was disassembled and reassembled as to break any wax film which may have formed during the precondition period. The purpose was to observe wax film formation during ozone exposure by use of the ozone rating system.

RESULTS AND DISCUSSION

Bloom Analysis - Wax Film Formation

Results from the bloom study are shown in figures 1 through 3. This data is the accumulated thickness of wax which formed on the surface of the sample over a twenty-one day period. It is of interest to note that the thickest film formation occurs at 22.5°C on all three wax samples. Film thickness was also higher at -20°C than at 65°C, the temperature extremes used in our study. This correlated extremely well with our ozone test results which will be discussed later. At 65°C, the wax film thickness was usually the best indicating increased wax solubility within the rubber matrix. The optimum bloom formation usually occurred around the 6th day. This is shown on the graphs by a decrease in slope. At most given times or temperatures, the strictly paraffin wax, wax C, had higher wax film formation on the rubber surface than either of the waxes containing a microcyrstalline portion.

Bloom Analysis - Surface Effects

One of the most interesting phenomena which was observed during the experimentation was the molecular weight distribution changes which occurred on the surface of the rubber vulcanizate. Figure 4 shows the molecular weight distribution of wax sample A. Figures 5 through 7 show the molecular weight distributions of wax A and the effects of temperature after 2, 11, and 21 days. Figures 8 through 15 contain the same information on waxes' B and C.

After 2 days, three general observations can be made as to changes occurring on the rubber surface. First the low molecular weight carbon species is in excess of that present in the original carbon distribution, indicating rapid surface migration of low molecular weight paraffin waxes. This phenomena also seems to be independent of temperature contrary to current belief. The second observation is that the overall molecular weight distribution tends to be the same as the original distribution. However, as mentioned above, the concentration of low molecular weight species is higher. Lastly, the high molecular weight ends, C-34 and above, did not vary much in concentration as compared to the original molecular weight distribution.

At 11 days, the rubber surface seems to be more stabilized. Good bell-shaped distributions have formed at all the test temperatures. The apex of the carbon distribution occurs around C-30. The high molecular carbon species remains about the same, whereas the low molecular weight species as are severely reduced in concentration compared to their 2 day counterparts. Again, this occurs independent of the test temperature.

The 21 day results show some minor destabilization as compared to the

11 day results with the exception of the surface conditions occurring at 23°C. The low molecular weight paraffins are again migrating, the pattern being random and independent of temperature. Broad, bell shaped distributions are observed on all the waxes at 23°C. An unpredictable change from original distribution has occurred in wax samples A and B at 23°C. These waxes contain a microcrystalline portion which suggest that the role of microcrystalline in the wax blend may highly influence wax performance. The best ozone protection was obtained on all three waxes at 23°C which will be discussed later.

Ozone Testing - Experimental Design

Due to the overwhelming amount of data available to be statistically treated, the data presented herein contains the 48 hour test results. Tables V and VI contain the coded coefficients of each variable in the quadratic equation used for regression analysis, where $A_1 = (X_1 - 22.5)/30.1$ and $A_2 = (X_2 - 2.25)/1.59$. Tables VII and VIII contain the error analysis results.

The results from equation (1) were plotted in two different forms, two dimensional crack contour plots and three dimensional graphs, both showing the percentage of ozone crack growth. Figures 16 through 21 are the contour graphs, both static and dynamic for the three waxes. Comparison of the static results to the dynamic counterparts reveal little difference between the plots, showing that minor differences would occur on the three dimensional graphs. When comparing figure 16 (30% micro) with figure 18 (20% micro), wax A provides better low temperature ozone protection whereas wax B has better high temperature protection. The carbon distributions of paraffinic portions of these waxes however, suggest

just the opposite. It has been demonstrated[11,12] that the optimum temperature of migration is 20-30°C below the melting point for narrow cut paraffin waxes. Work carried out[11] shows a paraffin wax with a melt point of 50°C has a high bloom rate at 20°C than at 40°C. Although bloom rate and ozone protection are not related in the case of petroleum waxes, it is generally believed that faster film formation yields greater ozone protection. It seems, that the temperature relations do not hold true after some paraffin portion of the wax has been replaced with microcrystalline. The microcrystalline containing waxes do offer better high and low temperature ozone resistance than the wax not containing a microcrystalline portion when comparing figures 16 and 18 with figure 20.

The contour plots show that when no wax is added, ozone cracking is observed at all temperatures. Increasing the wax concentration to 2.5 phr increases the ozone protection, but offers little additional protection above 2.5 phr. Actually, a detrimental protection is observed when the wax is increased above 2.7 phr in the low temperature regions. The best protection is observed when the wax concentration is 2.5 phr.

The three dimensional graphs for the static ozone results are shown in figures 22 through 24. Though containing the same information as the contour plots, they offer a different perspective in viewing the data. Being more difficult to accurately abstract raw data, the three dimensional plots offer instant recognition of trends which occur. Within the temperature limits of this study, the wax offered ozone protection is far worse at the high temperature regions (65°C) than at the low regions (-20°C).

CONCLUSIONS

Results presented in the foregoing study have shown that the degree of ozone cracking is temperature dependent. Cracking is minimized at 23°C. Ozone cracking increases steadily from a minimum as temperatures approach extremes of -20°C and + 65°C with no maximums observed.

Concentration of wax relative to ozone resistance is also observed. At 0 phr wax, ozone cracking is observed at all temperatures with all three waxes. Increasing the concentration to 2.5 phr increases protection, but offers little additional protection above 2.7 phr.

Statistical analysis suggests that the three waxes evaluated did not differ significantly in ozone chamber crack resistance although some minor differences were observed. All three waxes tend to protect better at the lower temperatures than at the elevated temperatures. The presence of microcrystalline wax is thought to influence ozone protection secondarily.

ACKNOWLEDGMENTS

The authors would like to thank the personnel and rubber technicians at Akron Rubber Development Laboratory for their superior work and support the past two years. They are also indebted to Tejbans Kohli of the Lord Corporation for his expertise and guidance relative to the statistical design methods utilized. The financial support of the Crystal Corporation in Lansdale, PA. is gratefully acknowledged and appreciated.

REFERENCES

[1] F. H. Kendall and J. Mann, J. Polym. Sci., 19, 505 (1956).

[2] D. Bruck, H. Honigshofen, and L. Ruetz, Rubber Chem. Technol., 58, 728 (1985).

[3] R. P. Lattimer, J. Grianelos, H. E. Diem, R. W. Layer, and C. K. Rhee, Rubber Chem. Technol., 52, 823 (1979).

[4] R. G. Newton, J. Rubber Research, 14, 27 (1945).

[5] J. Menough, Rubber World, (200), 6, 14 (1989).

[6] Witco Bulletin 800, June 1985, Witco Corporation.

[7] J. K. Andries, C. K. Rhee, R. W. Smith, D. B. Ross, H. E. Diem, Rubber Chem. Technol. 52, 823 (1979).

[8] R. P. Lattimer, E. R. Hooser, R. W. Layer and C. K. Rhee, Ruber Chem. Technol., 56, 431 (1983).

[9] R. P. Lattimer, R. W. Layer and C. K. Rhee, Rubber Chem. Technol., 57, 1023 (1984).

[10] A. N. Gent, in "Science and Technology of Rubber," F.R. Eirich, Ed., Academic Press, New York, p. 450, ch. 10 (1978).

[11] F. Jowett, Elastomerics, 48, (Sept., 1979).

[12] P. J. Dimauro, H. L. Paris, and M. A. Fath, Ruabber Chem. Technol., 52, 973 (1979).

TABLE I

Composition of Black Sidewall Compound

SIR	50.0
Polybutadiene	50.0
Zinc Oxide	3.5
Stearic Acid	1.0
Carbon Black N-326	40.0
Santoflex 13	1.5
Wax	Variable
Santocure NS	1.0
Insoluble Sulfur (80)	2.0

TABLE II

Wax Composition

Wax Sample	Paraffin Content	Microcrystalline Content
A	70	30
B	80	20
C	100	0

TABLE III

Physical Properties

Wax Sample	DTA, ^{o}C	DSC, ^{o}C	Capillary Melt Point, ^{o}C
A	58	64.1	70
B	57	63.7	68
C	48	64.2	62

TABLE IV

Two Variable Central Composite Design

Experiment Number	Coded Levels X1	X2	Temperature, °C	Wax Concentration, phr
1	-1	-1	-7.6	0.66
2	+1	-1	52.6	0.66
3	-1	+1	-7.6	3.84
4	+1	+1	52.6	3.84
5	+1.414	0	65.0	2.25
6	-1.414	0	-20.0	2.25
7	0	1.414	22.5	4.50
8	0	-1.414	22.5	0.0
9	0	0	22.5	2.25
10	0	0	22.5	2.25
11	0.667	0.836	42.6	3.58
12	-0.238	1.042	15.3	3.91
13	-0.963	0.464	-6.5	2.99
14	-0.963	-0.464	-6.5	1.51
15	-0.238	-1.042	15.3	0.59
16	0.667	-0.836	42.6	0.92
17	1.069	0	54.6	2.25

TABLE V

Crack Regression Analysis Results (48 hour Dynamic)

Variable	Wax A Coefficients	Wax B Coefficients	Wax C Coefficients
A_0	11.094	14.035	-0.007
A_1	20.378	10.909	17.397
A_2	-25.470	-23.209	-19.144
A_{12}	5.497	-2.776	4.050
A_{11}	27.827	25.765	33.873
A_{22}	21.292	21.022	30.072

TABLE VI

Crack Regression Analysis Results (48 hour Dynamic)

Variable	Wax A Coefficients	Wax B Coefficients	Wax C Coefficients
A_0	9.704	15.428	-0.007
A_1	17.055	10.746	17.987
A_2	-24.845	-23.924	-18.731
A_{12}	3.129	-4.016	2.800
A_{11}	33.327	24.991	34.917
A_{22}	22.346	18.238	30.540

TABLE VII

Error Analysis Results (48 hour Static)

Wax Sample	S	R^2 Adjusted	F (Regression)
A	16.99	17.7	12.1
B	26.19	43.9	3.5
C	27.89	53.7	3.09

TABLE VIII

Error Analysis Results (48 hour Dynamic)

Wax Sample	S	R^2 Adjusted	F (Regression)
A	14.38	83.0	16.6
B	25.20	46.4	3.77
C	29.05	51.7	2.93

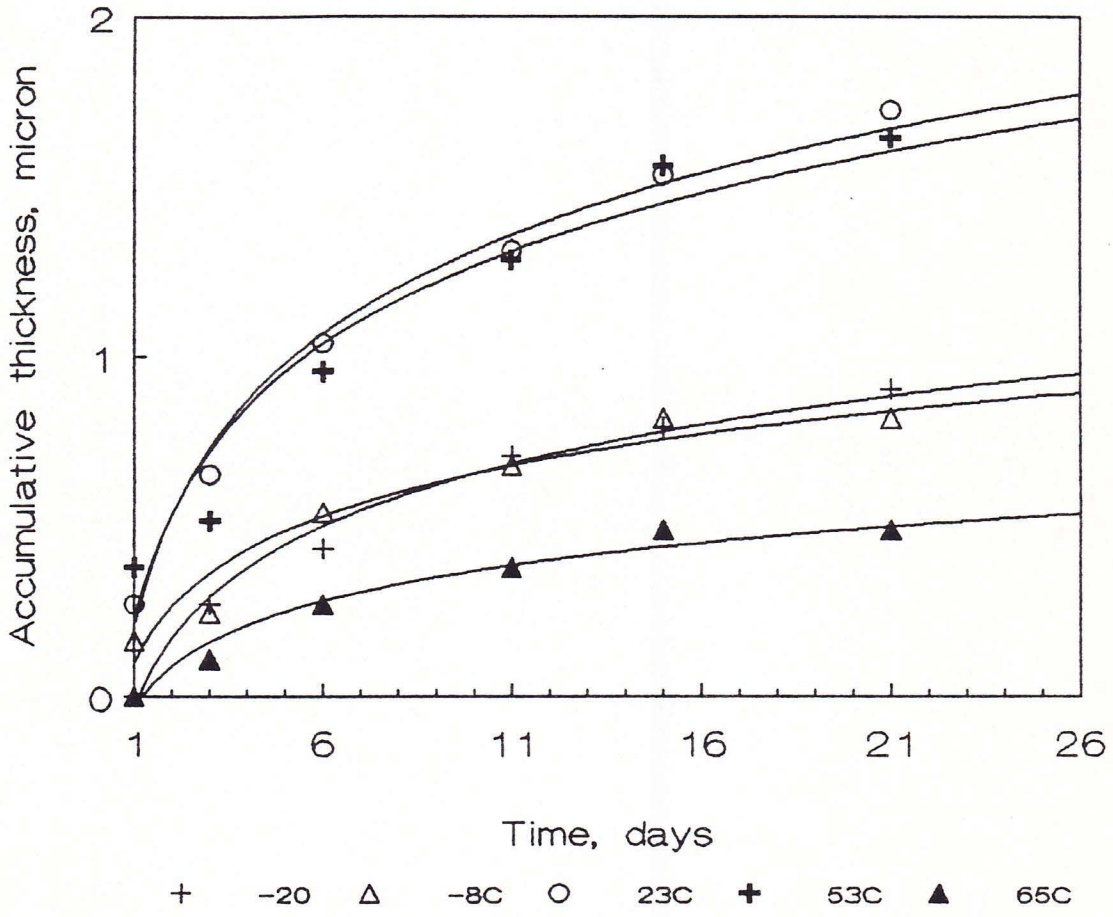

FIG. 1.——Bloom study of wax A.

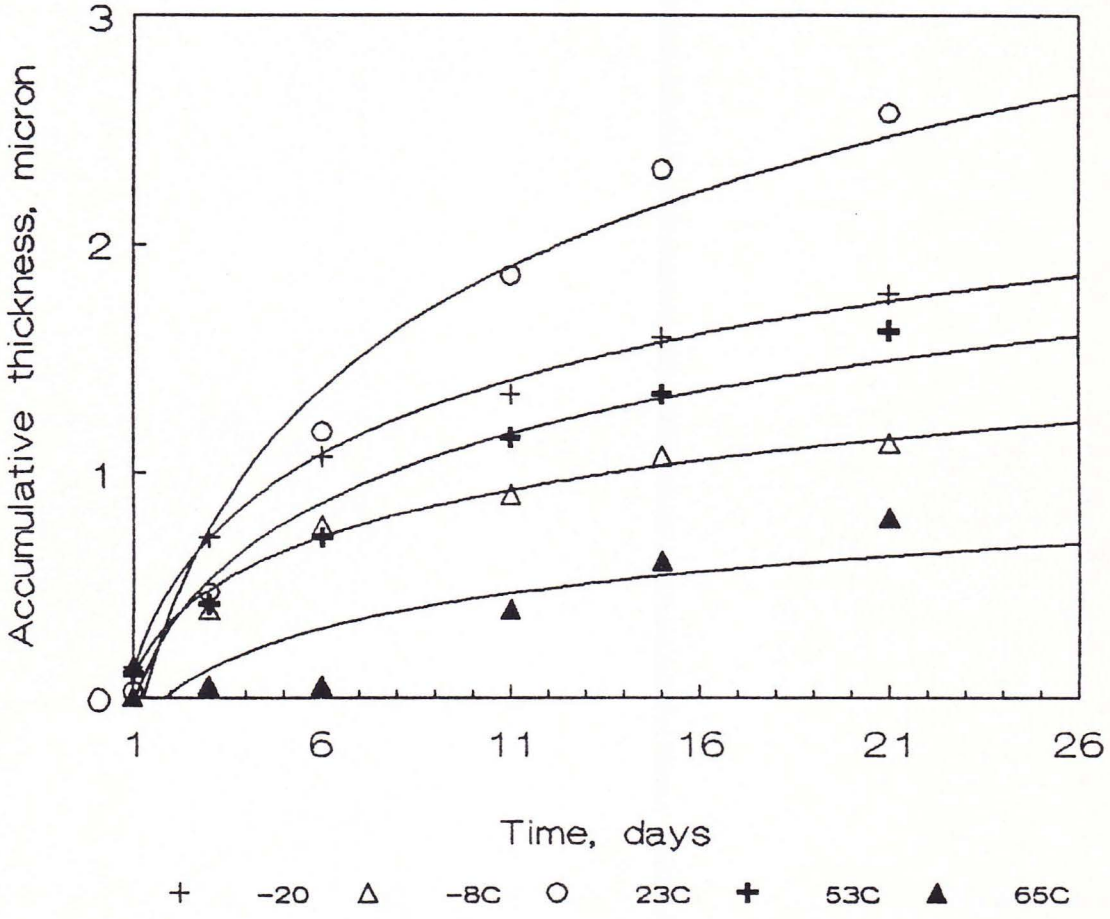

FIG. 2.——Bloom study of wax B.

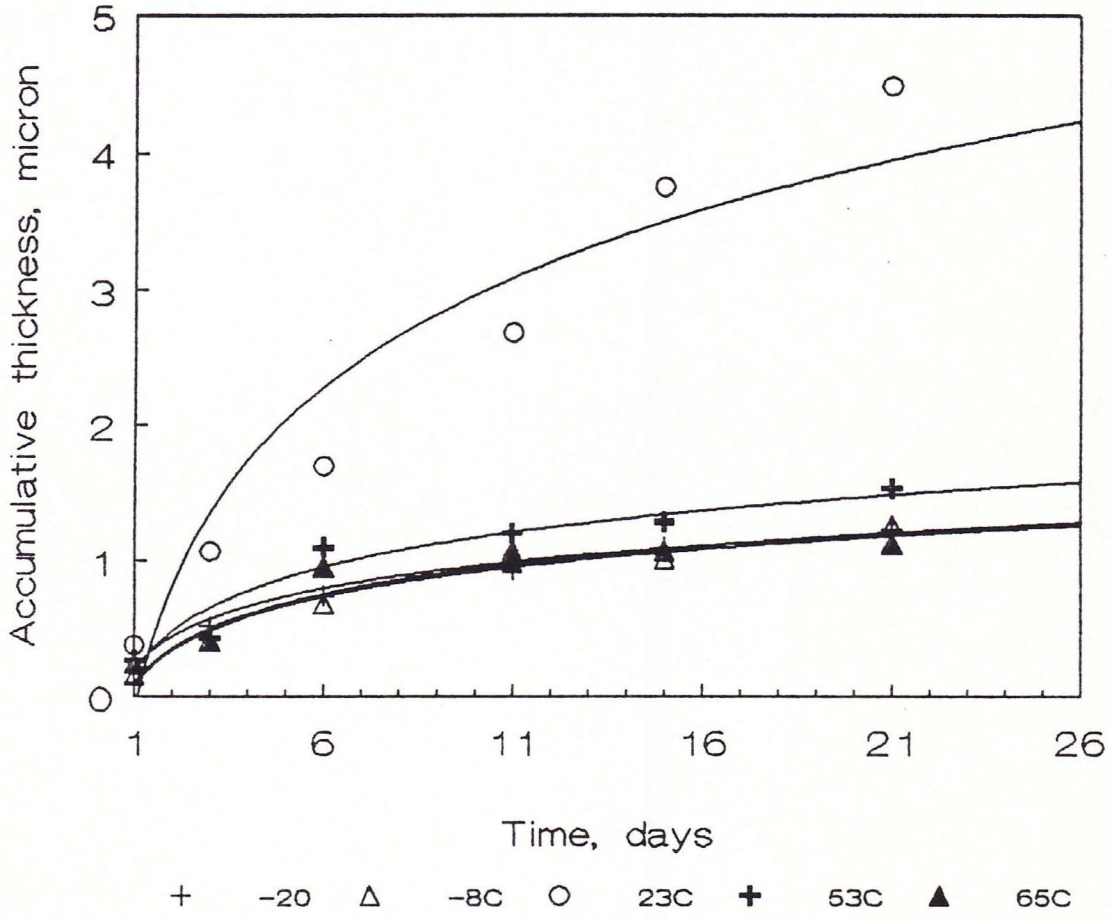

FIG. 3.——Bloom study of wax C.

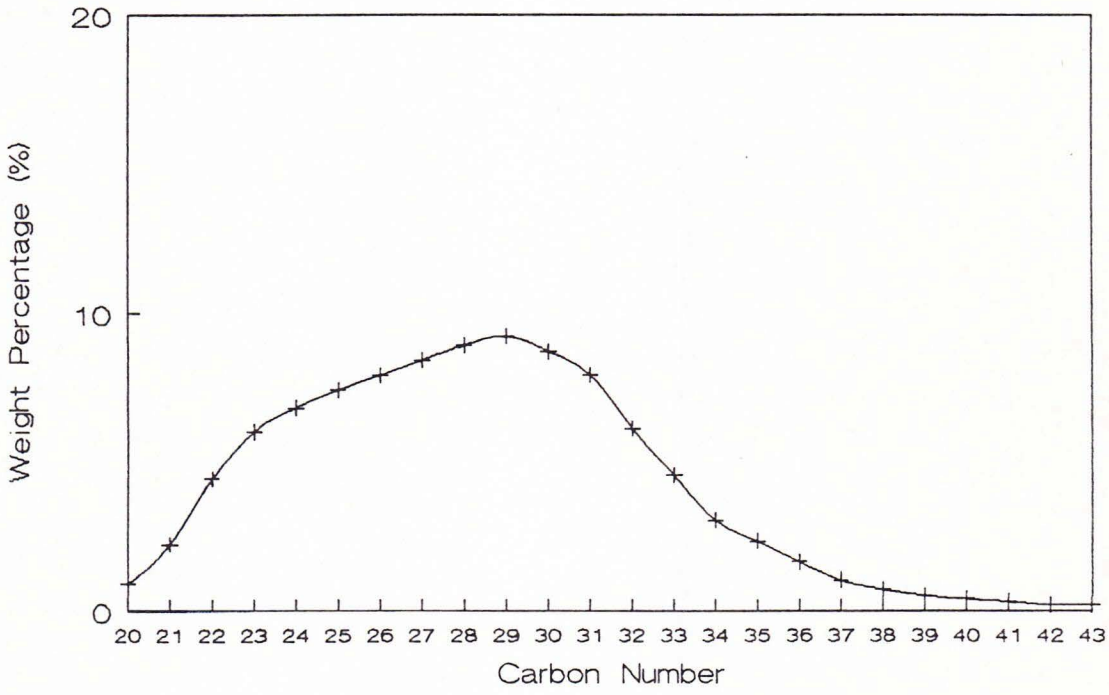

FIG. 4.——Molecular weight distribution of wax A.

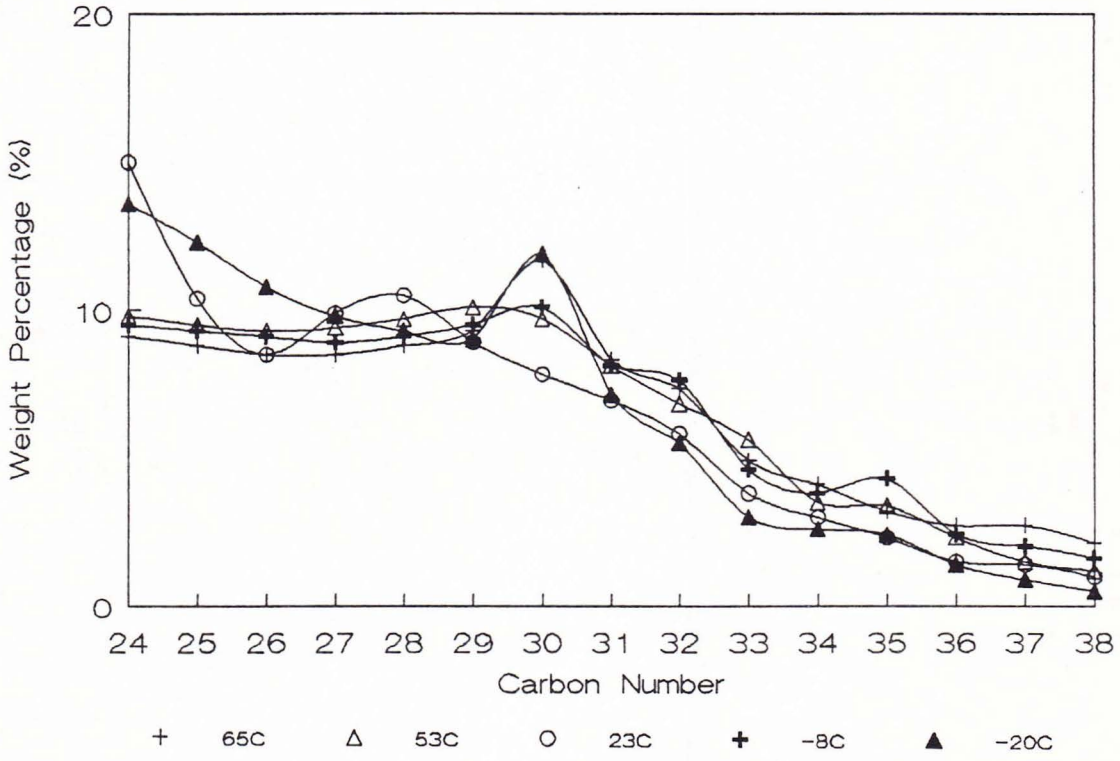

FIG. 5.——Temperature effect on molecular weight distribution on wax A after two days.

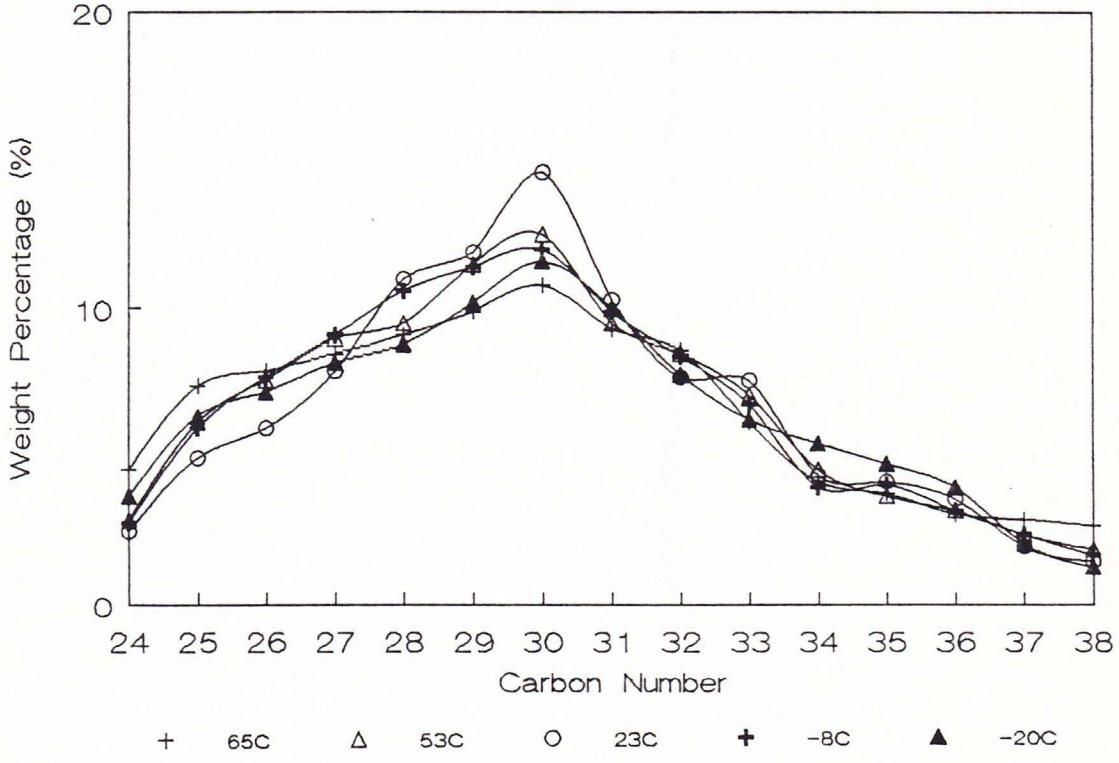

FIG. 6——Temperature effect on molecular weight distribution on wax A after eleven days.

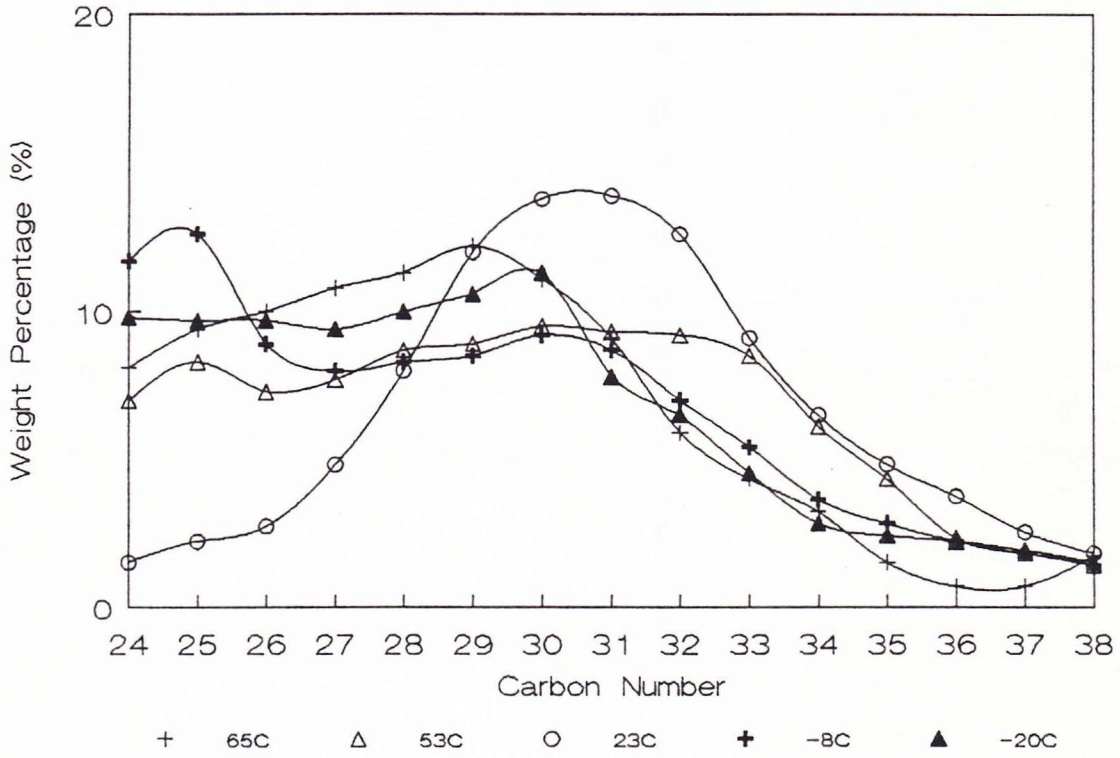

FIG. 7.——Temperature effect on molecular weight distribution on wax A after twenty-one days.

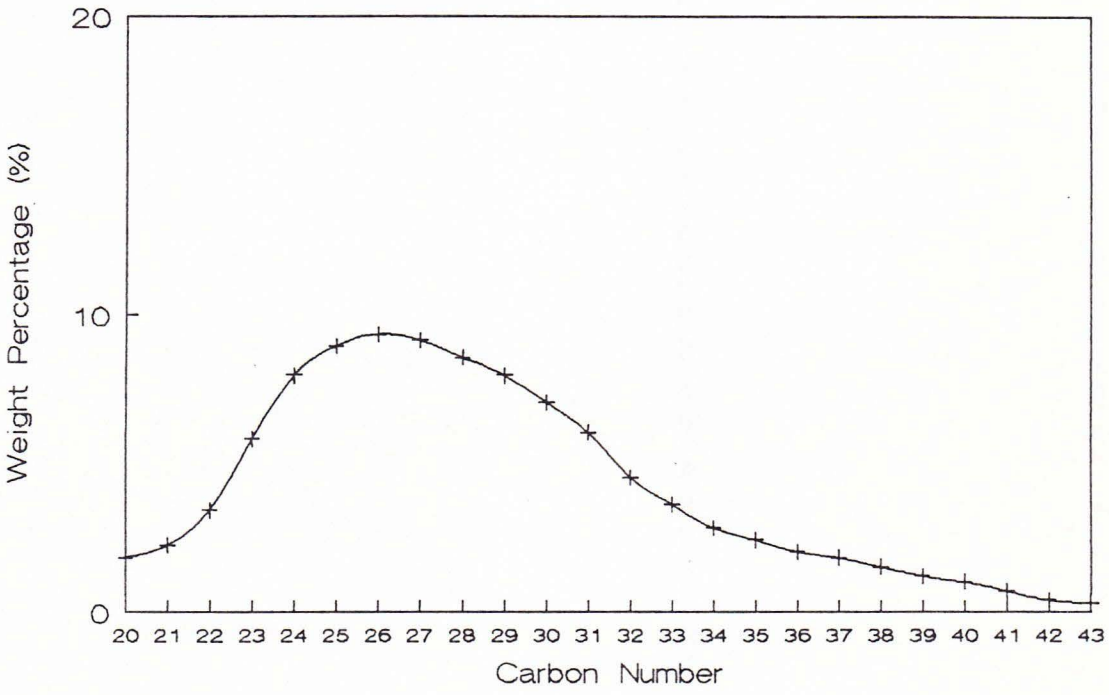

FIG. 8.——Molecular weight distribution of wax B.

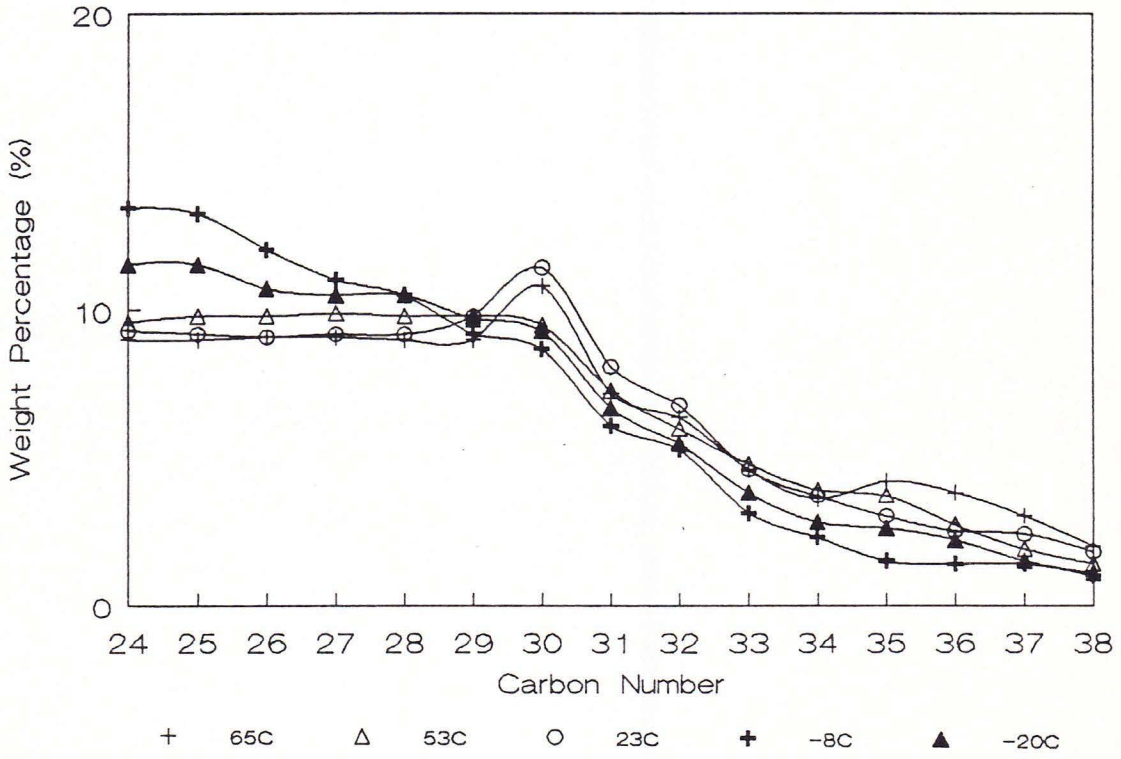

FIG. 9.——Temperature effect on molecular weight distribution on wax B after two days.

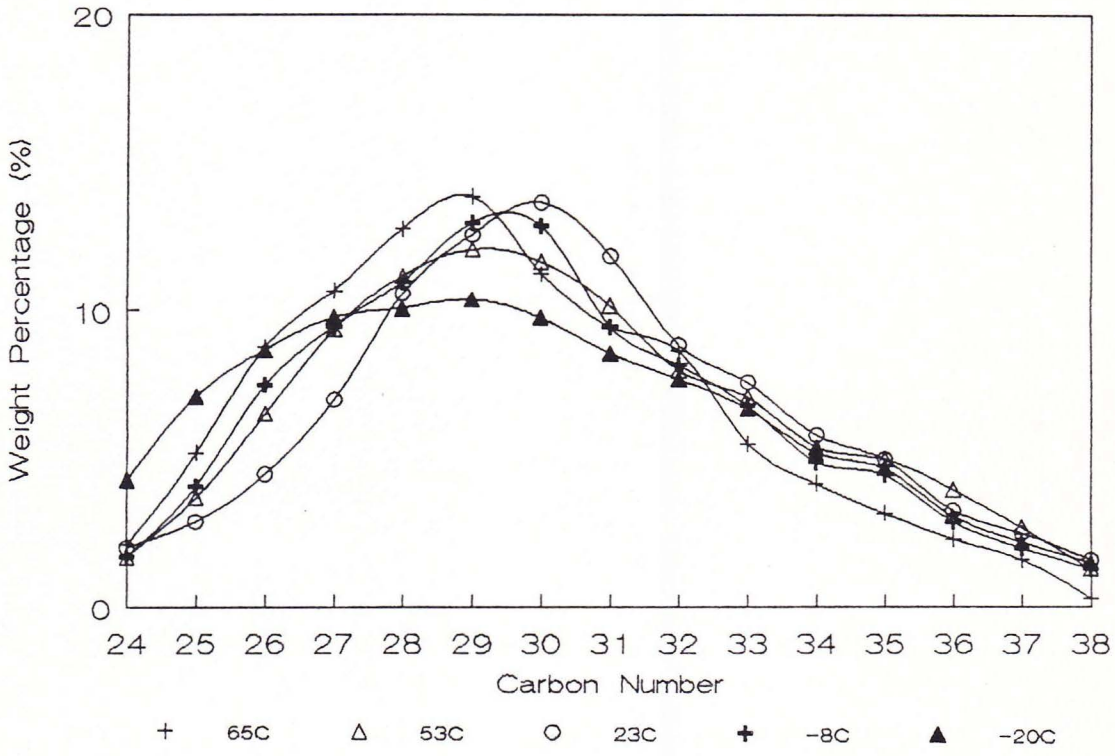

FIG. 10.——Temperature effect on molecular weight distribution on wax B after eleven days.

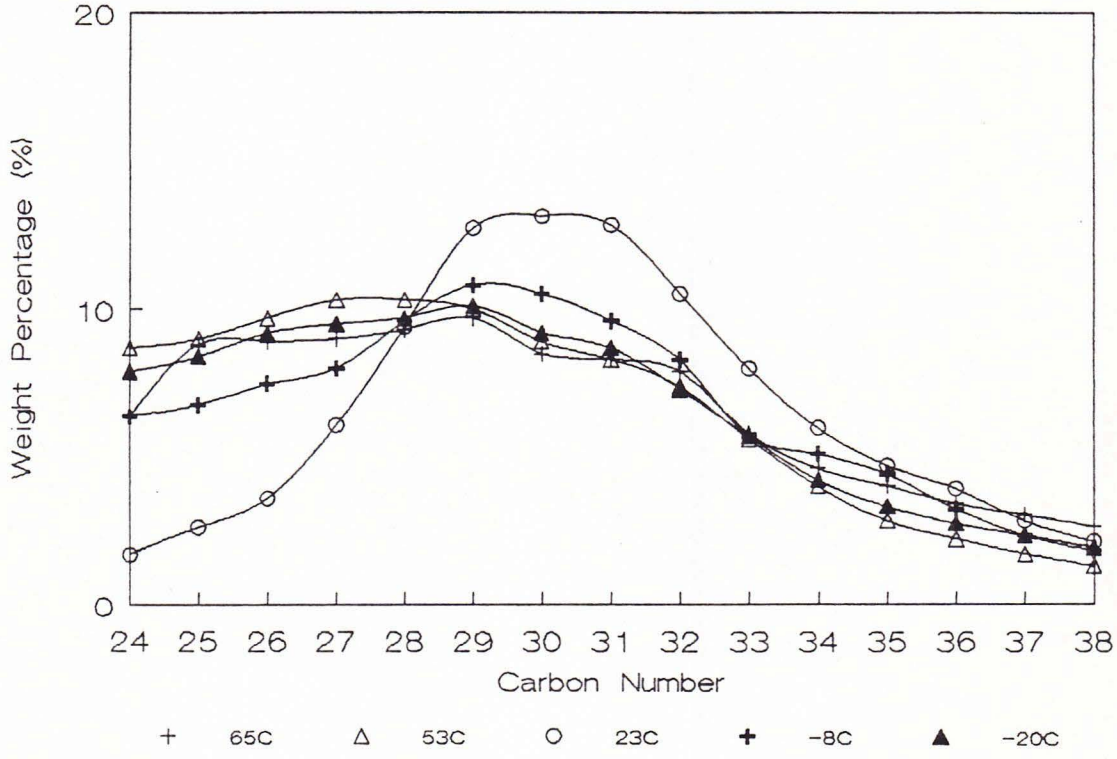

FIG. 11.——Temperature effect on molecular weight distribution on wax B after twenty-one days.

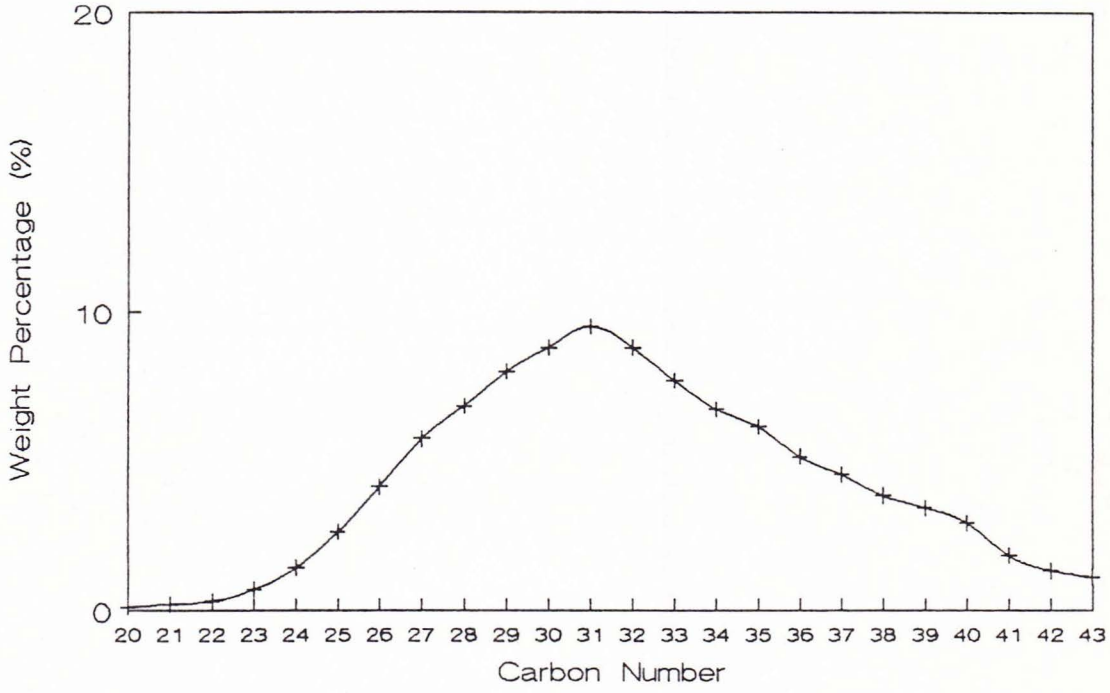

FIG. 12.——Molecular weight distribution of wax C.

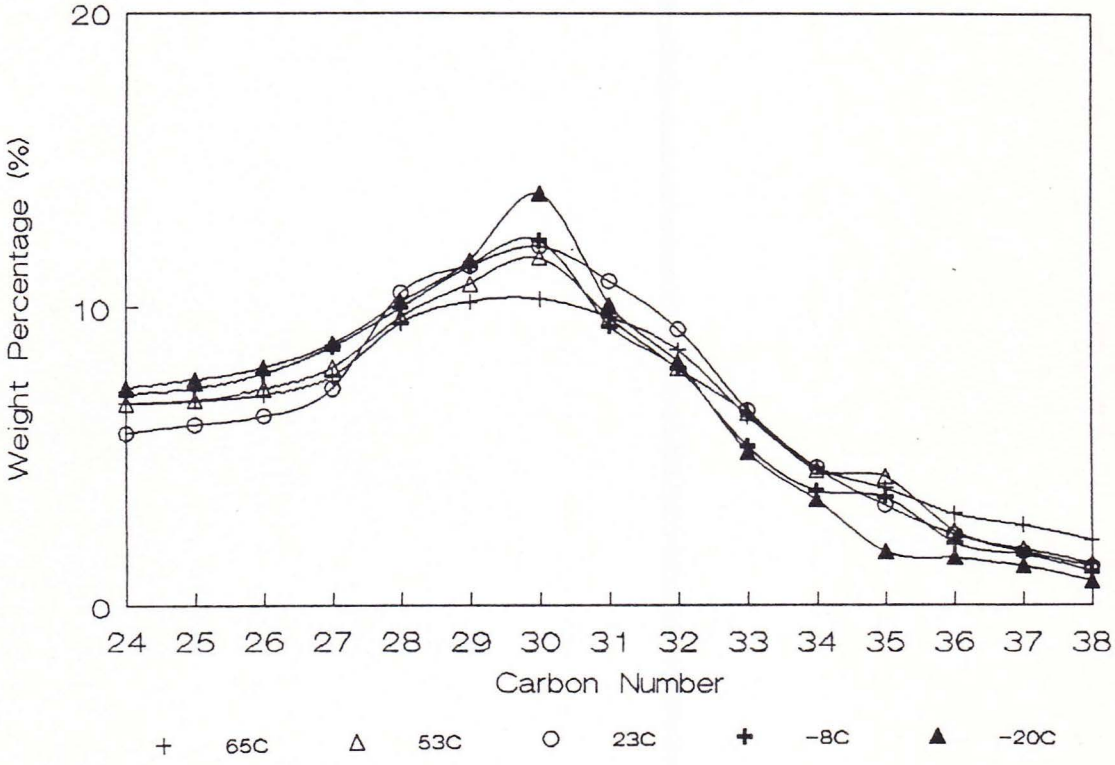

FIG. 13.——Temperature effect on molecular weight distribution on wax C after two days.

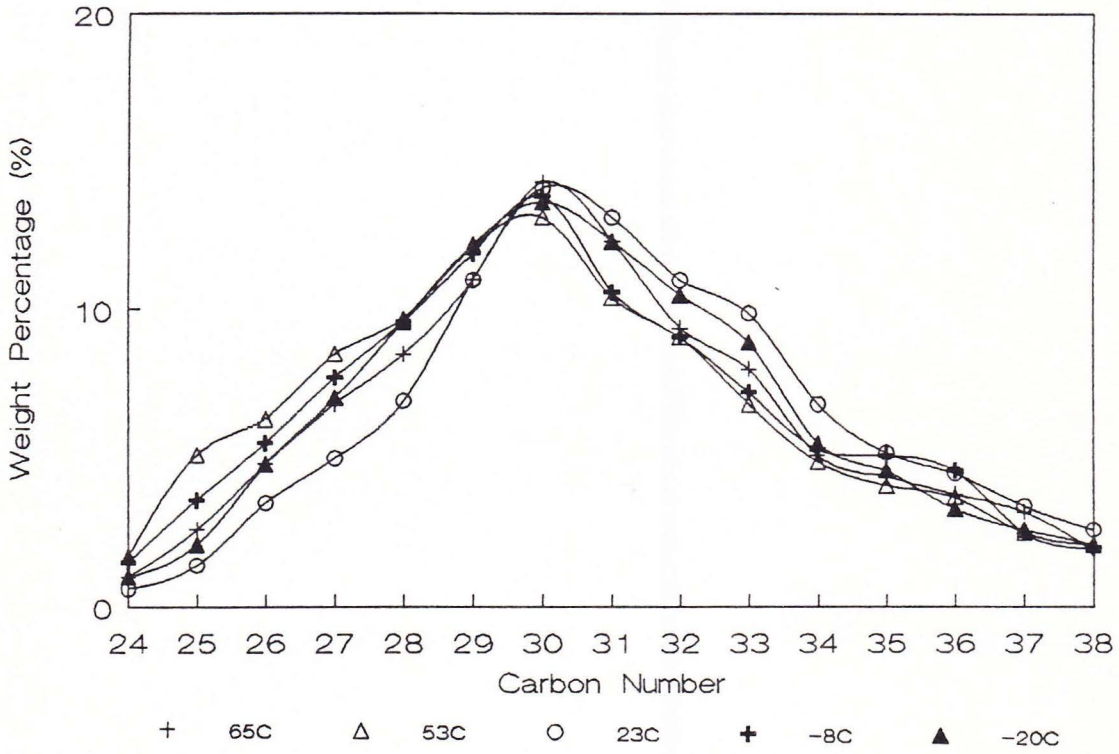

FIG. 14.——Temperature effect on molecular weight distribution on wax C after eleven days.

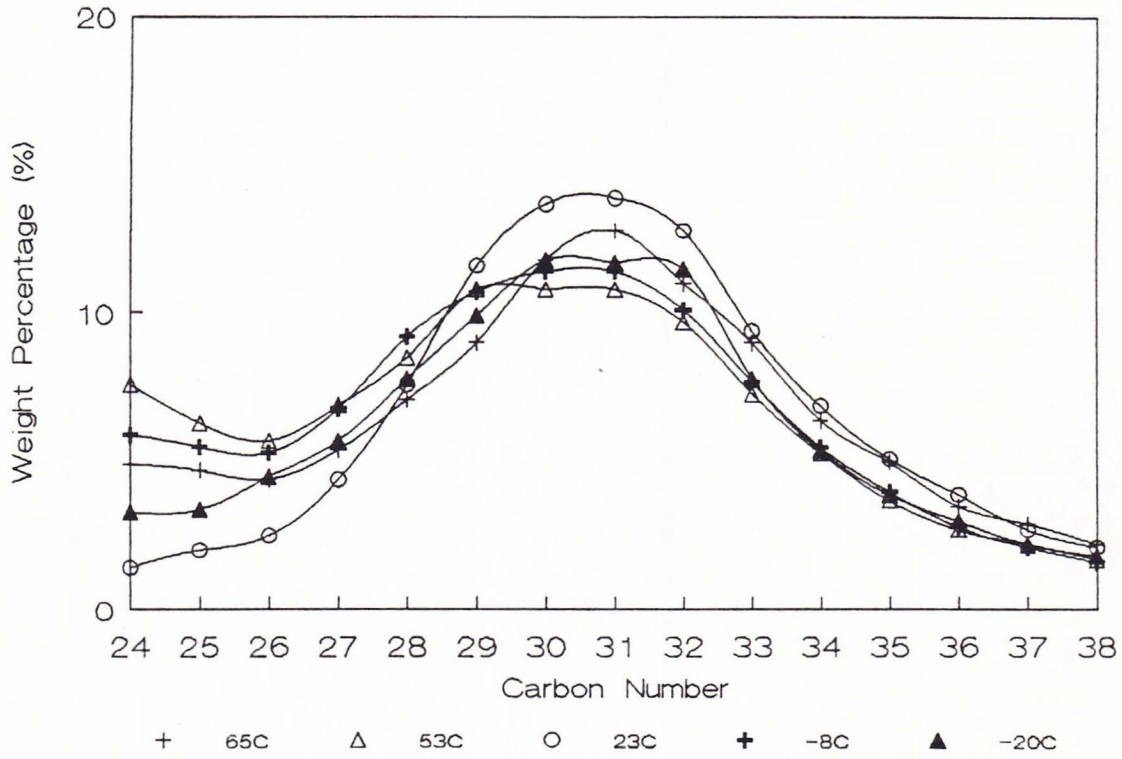

FIG. 15.——Temperature effect on molecular weight distribution on wax C after twenty-one days.

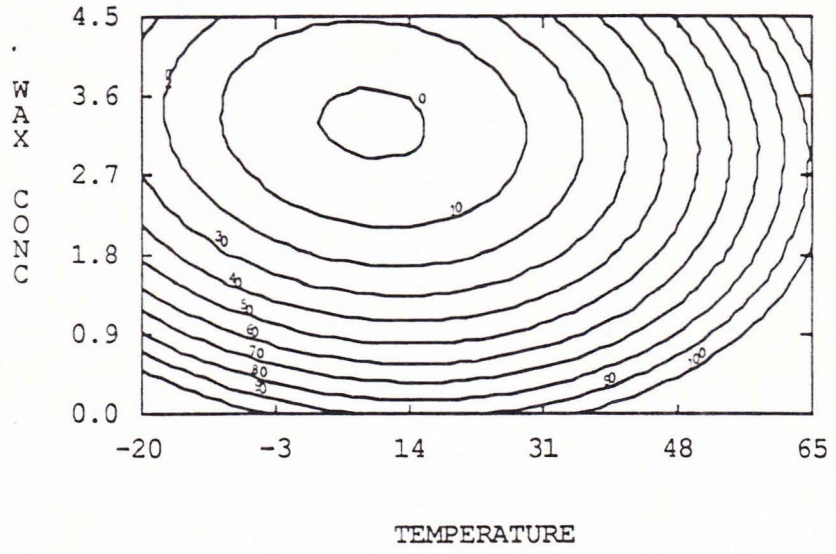

FIG. 16.——Crack contour for wax A (48 hour static).

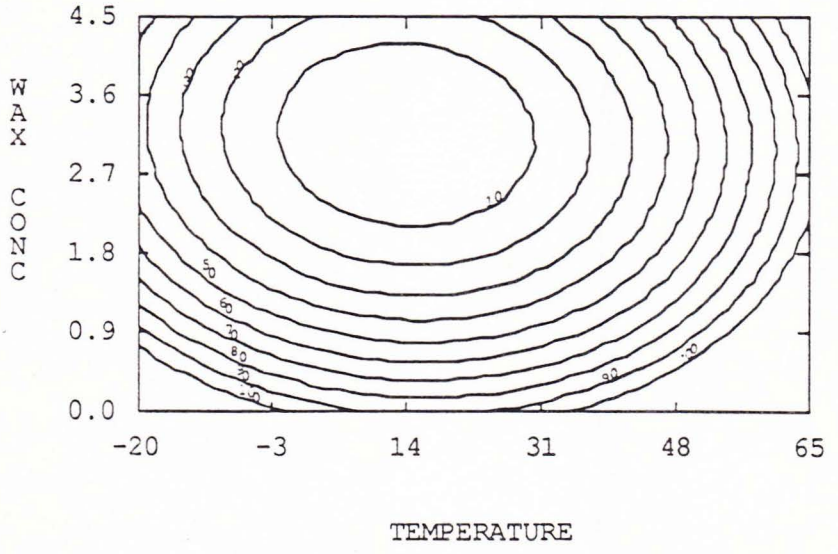

FIG. 17.——Crack contour for wax A (48 hour dynamic).

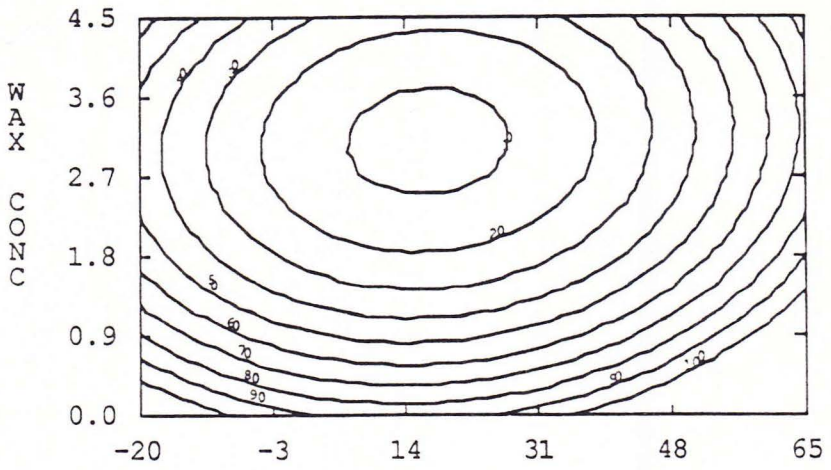

FIG. 18——Crack contour for wax B (48 hour static).

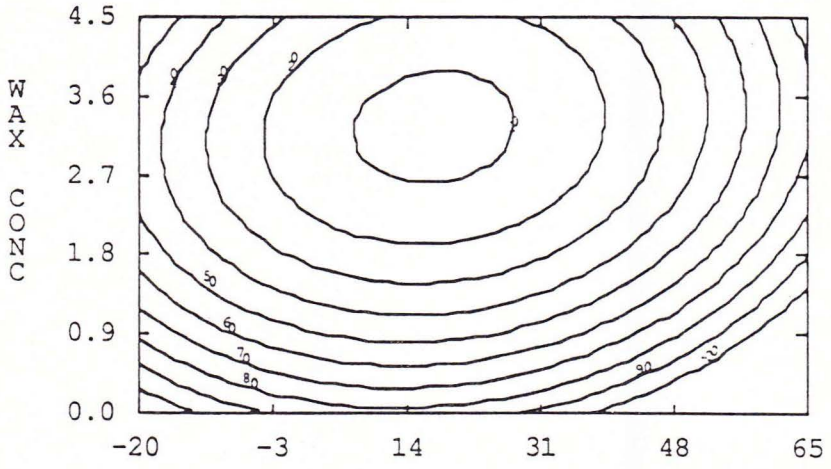

FIG. 19.——Crack contour for wax B (48 hour dynamic).

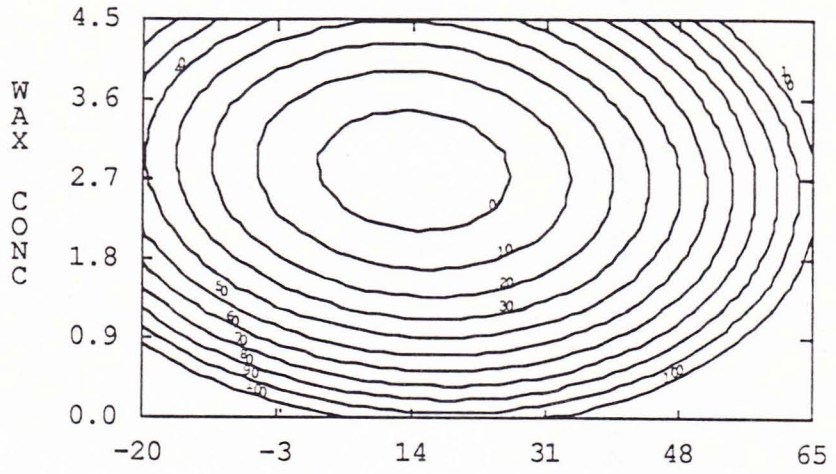

FIG. 20.——Crack contour for wax C (48 hour static).

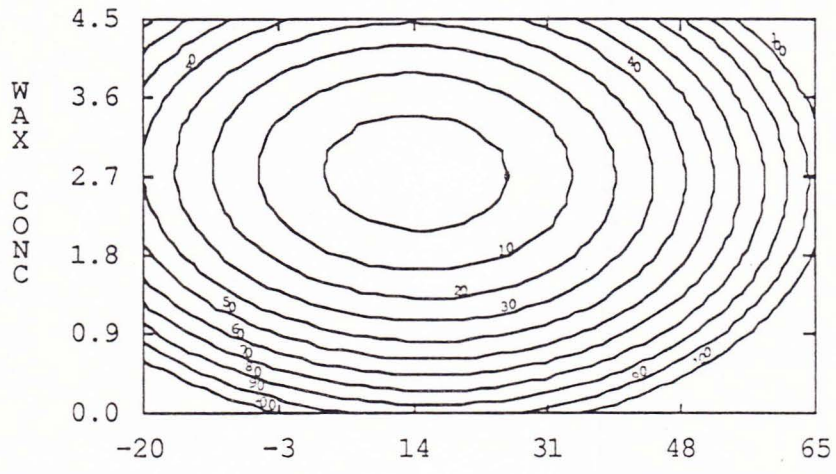

FIG. 21.——Crack contour for wax C (48 hour dynamic).

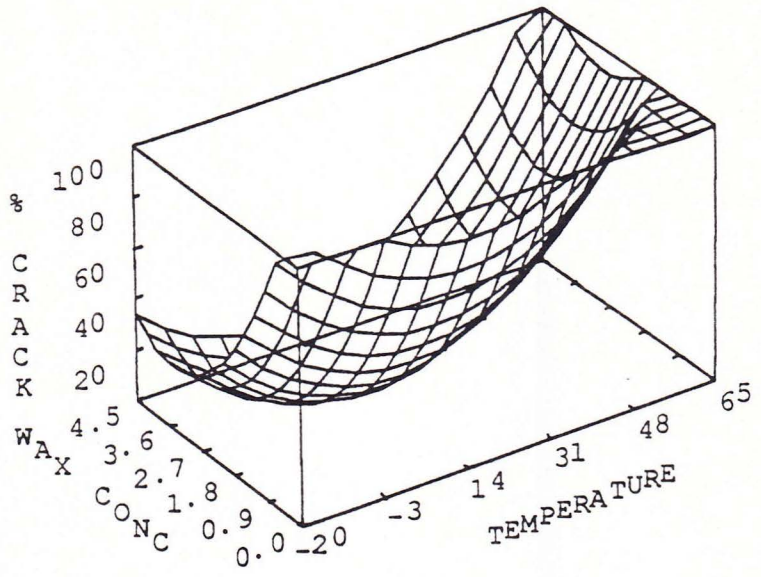

FIG. 22.——Crack response surface for wax A (48 hour static).

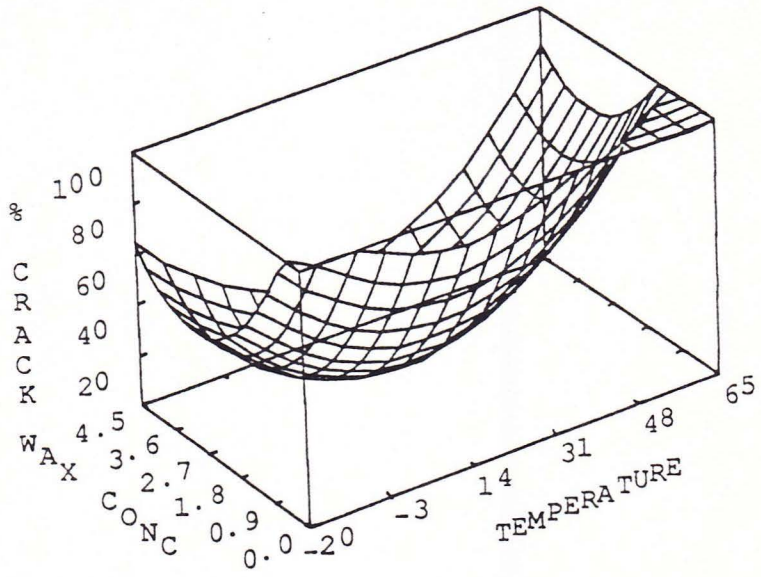

FIG. 23.——Crack response surface for wax B (48 hour static).

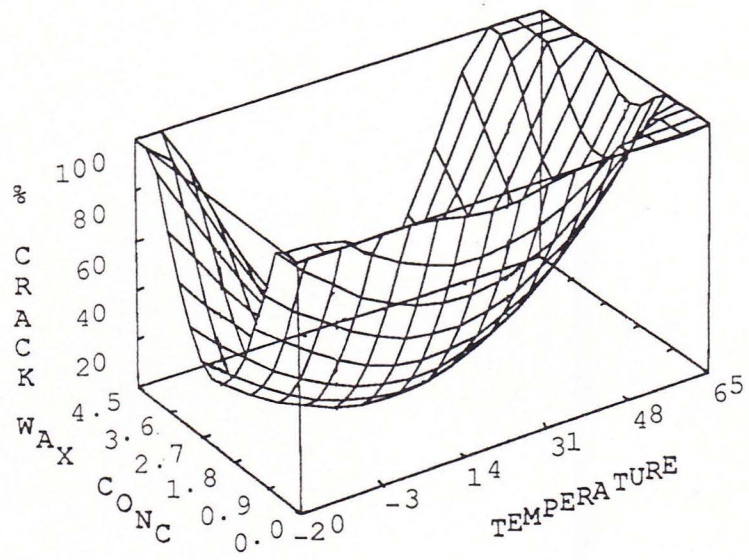

FIG. 24.——Crack response surface for wax C (48 hour static).